

Adaptive Symptom-Querying Strategy for Model-Based Personalized Prediction of Motion Sickness

Van Trong Dang¹, Takahiro Wada^{1*}

¹Human Robotics Laboratory, Division of Information Science, Nara Institute of Science and Technology, Ikoma, Nara, Japan

*** Correspondence:**

Takahiro Wada

t.wada@is.naist.jp

Keywords: Adaptive symptom-querying strategy, motion sickness, personalized symptom progression, computational model, subjective vertical conflict theory

Abstract

Personalized computational models based on subjective vertical conflict theory have been widely studied to predict or quantify motion sickness, providing a foundation for mitigating associated discomfort symptoms. However, frequent queries of passenger status at short intervals (e.g., one minute) may exacerbate motion sickness symptoms while simultaneously increasing the computational burden of the model. The present study proposes an adaptive querying strategy for acquiring passengers' symptom progression in terms of the Motion Illness Symptoms Classification (MISC), enabling sequential identification of personalized model parameters and prediction of future MISC values. Specifically, a query is issued when the model-predicted MISC, taking prediction uncertainty into account, reaches the next MISC level, or when a five-minute interval of motion exposure has elapsed. The collected MISC is then used to update the model parameters for subsequent predictions. The proposed approach is validated using a dataset obtained from participants exposed to linear lateral motion in darkness. The results demonstrate that the proposed strategy can successfully capture motion sickness progression trends while substantially reducing both the frequency of queries and the associated computational workload compared with conventional querying at one- or two-minute intervals.

1 Introduction

Recent advances in technologies used in ground transportation, the increasing use of in-vehicle devices, and the rapid spread of immersive virtual reality environments have made motion environments more complex, thereby elevating the likelihood of motion sickness (Golding & Gresty, 2005). For example, the emergence of automated driving systems has further increased this risk (Diels & Bos, 2016; Sivak & Schoettle, 2015; Wada, 2016), primarily as a result of (1) the shift from active driving to passive riding, i.e., the loss of vehicle control by occupants (Diels & Bos, 2016; Sivak & Schoettle, 2015), (2) changes in vehicle interior design such as seat orientation and layout (Diels & Bos, 2016), (3) alterations in vehicle motion characteristics (Wada, 2016; Yunus et al., 2025), and (4) the increased engagement in non-driving subtasks (Diels & Bos, 2016; Sivak & Schoettle, 2015). In view of this situation, the development of effective countermeasures against motion sickness has become a critical issue, and prediction technologies are expected to play a central role in this effort.

Various approaches have been proposed to predict motion sickness, among which computational modeling has been particularly well studied in recent years. One line of research focuses on fitting models, such as Motion Sickness Dose Value (MSDV) (ISO2631-1, 1997), which describe the relationship between body motion (in vertical) and sickness incidence based on empirical exposure–response data such as McCauley et al. (1976). Notably, this model has been officially validated for motion sickness induced by vertical motion without visual stimulation, and thus its extension to other sensory conditions has been pursued (Bos et al., 2024). Another line of research aims to capture the underlying mechanisms that explain how motion sickness occurs. The pioneering work by Oman (1982, 1990) is based on neural mismatch theory (Reason, 1978), which postulates that motion sickness develops when the mismatch between the integrated patterns of the sensory signals and the expected ones generated from the central nervous system (CNS). Furthermore, the pioneering computational work for quantitatively predicting motion sickness incidence (MSI) (McCauley et al., 1976), defined as the percentage of people who would vomit, was conducted by Bos & Bles (1998). This computational model is based on the subjective vertical conflict (SVC) or subjective vertical mismatch (SVM) theory (Bles et al., 1998), which postulates that motion sickness develops when there is a mismatch between the integrated sensed vertical direction derived from sensory signals and the expected vertical direction generated by the internal model thought to be built in the CNS. This SVC hypothesis can be regarded as a refined version of the neural mismatch theory. It should be noted that this pioneering model was the first to reproduce the phenomenon that MSI exhibits its peak around 0.2 Hz as observed in McCauley et al. (1976). Inspired by this original model (Bos & Bles, 1998) focused on vertical motion, various expanded versions of the SVC models have been developed, for example increasing the degrees of freedom of motion to account for otolith–canal interactions (Bos et al., 2002; Inoue et al., 2023; Kamiji et al., 2007; Wada et al., 2018; Wada & Bos, 2025). Furthermore, models incorporating visual information (Braccesi et al., 2011; Liu et al., 2024; Tamura et al., 2023; Wada et al., 2020) and addressing the effect of human motion predictability on motion sickness (Kuiper et al., 2019) have also been proposed (Wada, 2021). More recently, SVC models have been expanded to predict the progression of motion sickness symptoms, rather than MSI, in response to increasing demands for practical applications. For example, models to predict the Motion Illness Symptoms Classification (originally called the MIsery Scale, MISC) (Bos et al., 2005), an 11-point subjective rating scale based on the progression of symptoms, have been developed (Inoue et al., 2024, 2025; Kotian et al., 2023, 2025; Yunus et al., 2022), inspired by a similar attempt with a model based on the neural mismatch theory (Irmak et al., 2022). Furthermore, Inoue et al. (2025) demonstrated that the symptom progression described by MISC for each individual can be predicted using model parameters identified from past observations of MISC and head motion.

Although the aforementioned SVC models successfully predict the symptom progression of individuals, several issues remain when applying them to engineering applications. One of these issues concerns how to obtain motion sickness data. In the present study, we assume that symptom progression data, such as MISC, can be sequentially obtained and used for online model parameter identification to predict individual symptom progression, based on previous findings (Inoue et al., 2025), which demonstrated that model accuracy improves as more data become available. In conventional studies investigating the characteristics of motion sickness, MISC scores were typically obtained at regular intervals, such as every minute (Irmak, Pool, et al., 2021; Kuiper et al., 2020; Sato et al., 2026). However, in future engineering applications, it may not always be feasible to collect such subjective ratings frequently. Repeated questioning could degrade the user experience, and it might even affect the subjective ratings themselves, potentially leading to either under- or overestimation of motion sickness. Therefore, we formulated the idea of reducing the sampling frequency of MISC measurements while preserving model accuracy.

The present study considers a situation in which the system occasionally queries users for their MISC ratings to sequentially identify model parameters and predict future symptom progression, given that head motion data are available. The purpose of the present study is to develop a method to determine the optimal timing for symptom queries, aiming to reduce their frequency while preserving model accuracy in such situations. Specifically, the method determines the timing for querying the MISC by predicting when MISC increases, accounting for the uncertainty in the model-predicted MISC. To validate the proposed method, we employ a dataset collected in experiments (Orita et al., 2025) in which participants were exposed to lateral motion under dark conditions without visual cues.

2 Method

2.1 Computational Model of Individual Symptom Progression of Motion Sickness

The present study employs the computational model of Inoue et al. (2025), which is based on the subjective vertical conflict (SVC) theory and represents the progression of motion sickness symptoms at the individual level (Fig. 1). The inputs to the model are the head angular velocity vector $\omega (\in R^3)$ and the gravito-inertial acceleration (GIA) $f (= g + a \in R^3)$, where g and a denote the gravitational and inertial acceleration vectors, respectively. The model output is the Motion Illness Symptoms Classification (MISC) score (Bos et al., 2005), which is a subjective measure of motion sickness symptom progression based on an 11-point scale. The model incorporates the dynamics of the otolith and semicircular canal sensory organs together with low-pass filtering to decompose f into the sensed vertical gravitational acceleration v_s and the sensed inertial acceleration a_s . This process is referred to as the generalized Mayne Equation (Bos & Bles, 2002). In addition, it is assumed that the human central nervous system (CNS) contains an internal model with identical dynamics, which is used to compute the expected gravitational acceleration \hat{v}_s , the expected inertial acceleration \hat{a}_s , as well as the expected angular velocity $\hat{\omega}_s$. The mismatch between the sensed and expected vertical gravitational accelerations, referred to as the subjective vertical conflict (SVC), $\Delta v (:= v_s - \hat{v}_s)$, is then calculated. The component of the model that performs these computations is referred to as the SVC part (Fig.1). In the MISC output part of the model, the SVC Δv is converted into the MISC score. The dynamic relationship between the SVC and the MISC score is modeled using a combination of a Hill function, which is defined as $u_i = \frac{(\|\Delta v\|/b)^2}{1 + (\|\Delta v\|/b)^2}$ with fast and slow pathways, which is referred to as OmanHLL in Inoue et al. (2024, 2025). It should be noted that Inoue et al. (2025) demonstrated that the observed progression of MISC scores at the individual level can be reproduced by tuning only the parameters $\theta := [b, K, \beta_1, \beta_2]^T$ in the MISC output part for each individual. For further details of the model structure and parameterization can be found in Inoue et al. (2025).

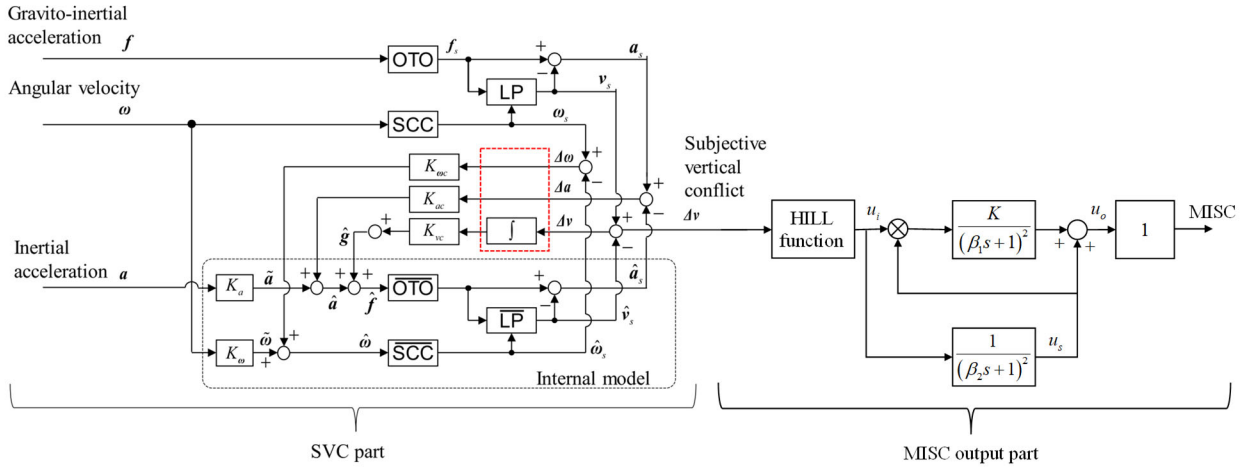


Figure 1. Computational model of motion sickness, consisting of the SVC part and the MISC output part.

2.2 Proposed Adaptive Symptom-Querying Strategies for Prediction

In this study, we consider a scenario in which online parameter identification of the 6DoF-SVC model is performed each time a participant's MISC score is obtained, and the future MISC progression for the same individual is subsequently predicted. Under this setting, an algorithm that reduces the number of MISC queries is proposed while maintaining sufficient model prediction accuracy.

First, the optimal parameters of the MISC output part are identified using the currently available observation data as follows:

$$\theta^* = [b^* \ K^* \ \beta_1^* \ \beta_2^*]^T = \arg \min_{\theta} J(\theta), \quad (1)$$

where the cost function is defined as $J(\theta) := \sum_{k=1}^N (MISC_k^{mdl}(\theta) - MISC_k^{obj})^2$. Here $MISC_k^{obs}$ and $MISC_k^{mdl}$ denote observed MISC value at the k -th query and its corresponding model prediction, respectively, and N denotes the number of data points currently available.

Second, parameter sets in the vicinity of the optimal parameter vector θ^* are sampled to quantify the uncertainty of the prediction. A second-order Taylor expansion of the cost function $J(\theta)$ around the optimal parameter vector θ^* yields

$$J(\theta) \approx J(\theta^*) + \left(\frac{\partial J(\theta)}{\partial \theta} \bigg|_{\theta=\theta^*} \right)^T (\theta - \theta^*) + \frac{1}{2} (\theta - \theta^*)^T \left(\frac{\partial^2 J(\theta)}{\partial \theta \partial \theta^T} \bigg|_{\theta=\theta^*} \right) (\theta - \theta^*). \quad (2)$$

At the optimal parameter vector θ^* , the following condition is necessarily satisfied:

$$\left(\frac{\partial J(\theta)}{\partial \theta} \bigg|_{\theta=\theta^*} \right)^T (\theta - \theta^*) = 0.$$

136 Substituting this condition into (2) yields

$$137 \quad J(\boldsymbol{\theta}) - J(\boldsymbol{\theta}^*) \approx \frac{1}{2}(\boldsymbol{\theta} - \boldsymbol{\theta}^*)^T \left(\frac{\partial^2 J(\boldsymbol{\theta})}{\partial \boldsymbol{\theta} \partial \boldsymbol{\theta}^T} \bigg|_{\boldsymbol{\theta}=\boldsymbol{\theta}^*} \right) (\boldsymbol{\theta} - \boldsymbol{\theta}^*). \quad (3)$$

138 Based on the local curvature of the parameter space characterized by the Hessian matrix in (3), the
 139 MISC output part parameters ($\boldsymbol{\theta}$) sampled in the vicinity of the optimal parameter set ($\boldsymbol{\theta}^*$) are
 140 assumed to lie within the following domain:

$$141 \quad S = \left\{ \boldsymbol{\theta} \in \mathbb{R}_+^4 \mid (\boldsymbol{\theta} - \boldsymbol{\theta}^*)^T \left(\frac{\partial^2 J(\boldsymbol{\theta})}{\partial \boldsymbol{\theta} \partial \boldsymbol{\theta}^T} \bigg|_{\boldsymbol{\theta}=\boldsymbol{\theta}^*} \right) (\boldsymbol{\theta} - \boldsymbol{\theta}^*) \leq 2\delta \right\}, \quad (4)$$

142 where δ denotes an acceptable tolerance.

143 Computing the Hessian matrix

$$144 \quad \mathbf{H} = \frac{\partial^2 J(\boldsymbol{\theta})}{\partial \boldsymbol{\theta} \partial \boldsymbol{\theta}^T} \bigg|_{\boldsymbol{\theta}=\boldsymbol{\theta}^*} = [H_{ij}] \in \mathbb{R}^{4 \times 4}$$

145 poses significant challenges, particularly in the case of high-dimensional cost functions. Therefore,
 146 to reduce the computational complexity associated with evaluating the Hessian, a simple
 147 approximation based on the Taylor expansion is employed as follows:

$$148 \quad H_{ij} = \frac{\partial^2 J}{\partial \theta_i \partial \theta_j} = \frac{J_1^{ij} - J_2^{ij} - J_3^{ij} + J_4^{ij}}{4\varepsilon^2}, \quad (5)$$

149 where ε is the differential step size. The terms $J_1^{ij}, J_2^{ij}, J_3^{ij}$ and J_4^{ij} are defined as follows:

$$150 \quad J_1^{ij} := J(\boldsymbol{\theta}^* + \varepsilon \mathbf{I}_i + \varepsilon \mathbf{I}_j) = J(\boldsymbol{\theta}^*) + \varepsilon \frac{\partial J}{\partial \theta_i} + \varepsilon \frac{\partial J}{\partial \theta_j} + \frac{\varepsilon^2}{2} \frac{\partial^2 J}{\partial \theta_i \partial \theta_i} + \varepsilon^2 \frac{\partial^2 J}{\partial \theta_i \partial \theta_j} + \frac{\varepsilon^2}{2} \frac{\partial^2 J}{\partial \theta_j \partial \theta_j}, \quad (6)$$

$$151 \quad J_2^{ij} := J(\boldsymbol{\theta}^* - \varepsilon \mathbf{I}_i + \varepsilon \mathbf{I}_j) = J(\boldsymbol{\theta}^*) - \varepsilon \frac{\partial J}{\partial \theta_i} + \varepsilon \frac{\partial J}{\partial \theta_j} + \frac{\varepsilon^2}{2} \frac{\partial^2 J}{\partial \theta_i \partial \theta_i} - \varepsilon^2 \frac{\partial^2 J}{\partial \theta_i \partial \theta_j} + \frac{\varepsilon^2}{2} \frac{\partial^2 J}{\partial \theta_j \partial \theta_j}, \quad (7)$$

$$152 \quad J_3^{ij} := J(\boldsymbol{\theta}^* + \varepsilon \mathbf{I}_i - \varepsilon \mathbf{I}_j) = J(\boldsymbol{\theta}^*) + \varepsilon \frac{\partial J}{\partial \theta_i} - \varepsilon \frac{\partial J}{\partial \theta_j} + \frac{\varepsilon^2}{2} \frac{\partial^2 J}{\partial \theta_i \partial \theta_i} - \varepsilon^2 \frac{\partial^2 J}{\partial \theta_i \partial \theta_j} + \frac{\varepsilon^2}{2} \frac{\partial^2 J}{\partial \theta_j \partial \theta_j}, \quad (8)$$

$$153 \quad J_4^{ij} := J(\boldsymbol{\theta}^* - \varepsilon \mathbf{I}_i - \varepsilon \mathbf{I}_j) = J(\boldsymbol{\theta}^*) - \varepsilon \frac{\partial J}{\partial \theta_i} - \varepsilon \frac{\partial J}{\partial \theta_j} + \frac{\varepsilon^2}{2} \frac{\partial^2 J}{\partial \theta_i \partial \theta_i} + \varepsilon^2 \frac{\partial^2 J}{\partial \theta_i \partial \theta_j} + \frac{\varepsilon^2}{2} \frac{\partial^2 J}{\partial \theta_j \partial \theta_j}, \quad (9)$$

154 in which $\mathbf{I}_i \in \mathbb{R}^4$ and $\mathbf{I}_j \in \mathbb{R}^4$ denote the i -th and j -th standard basis vectors, respectively, i.e., vectors
 155 with a value of 1 at the i -th or j -th entry and 0 elsewhere. Accordingly, M parameter sets can be
 156 generated by sampling from the set defined by (4), yielding M corresponding predicted MISC values.

157 From this predicted MISC data, we can calculate the mean predicted MISC in the following
158 formulation.

$$159 \quad \overline{\text{MISC}}^P(t) = \frac{1}{M} \sum_{l=1}^M \text{MISC}_l^P(t), \quad (10)$$

160 where $\text{MISC}_l^P(t)$ is the predicted MISC at the l -th sample among M total samples. In addition, the
161 predicted uncertainty can be quantified from the standard deviation of the predicted MISC scores as
162 follows:

$$163 \quad \text{SD}(t) = \sqrt{\frac{1}{M-1} \sum_{l=1}^M \left(\text{MISC}_l^P(t) - \overline{\text{MISC}}^P(t) \right)^2}. \quad (11)$$

164 Based on the formulations described above, we propose an algorithm that determines when symptom
165 querying should be performed to update model parameters, while the model continuously predicts
166 future MISC progression, as illustrated in Fig. 2. As the first criterion, MISC querying is performed at
167 the time point when the model-predicted MISC, accounting for prediction uncertainty, is expected to
168 exceed the previously observed MISC by one or more levels, that is, when condition (12) is satisfied.

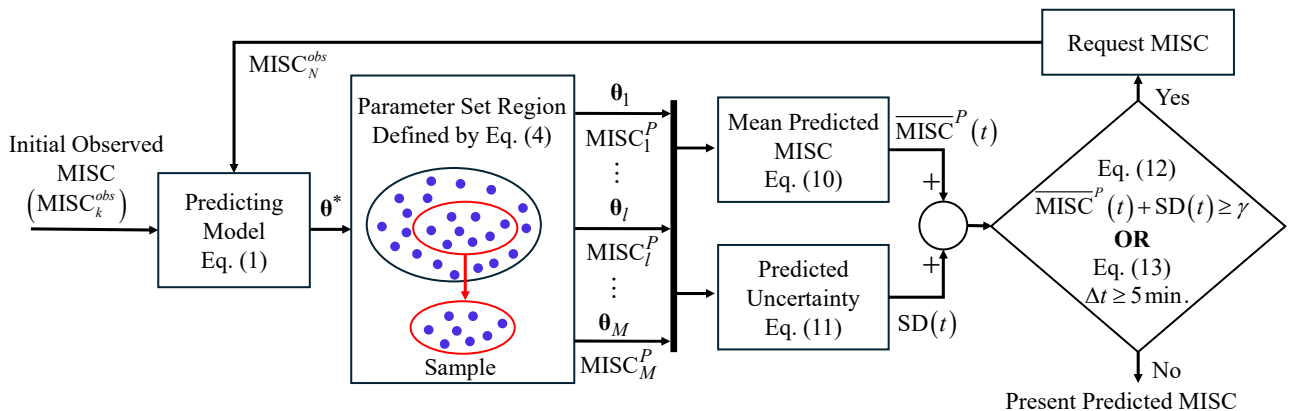
$$169 \quad \overline{\text{MISC}}^P(t) + \text{SD}(t) \geq \gamma = \text{MISC}_N^{\text{obs}} + 1, \quad (12)$$

170 where $\text{MISC}_N^{\text{obs}}$ denotes the last observed MISC from the current collected data.

171 Although this strategy effectively reduces unnecessary queries, it inherently relies too heavily on the
172 model's instantaneous accuracy, making the system vulnerable to prediction errors. To mitigate this,
173 we introduce an additional timing-based rule, which queries the passenger's MISC after a 5-minute
174 interval of motion exposure, as follows:

$$175 \quad \Delta t = t - t_{\text{last}} \geq 5 \text{ min.}, \quad (13)$$

176 in which t_{last} is the last time of querying MISC. Thus, the strategy queries the MISC score either when
177 the condition in (12) is satisfied or when the 5-minute interval of motion exposure has elapsed. This
178 hybrid mechanism ensures that the model can still query through (12), while the timing-based rule
179 prevents indefinite inactivity caused by potential model inaccuracies.



180

Figure 2. Overview of the proposed strategy for adaptive symptom querying and personalized prediction of motion sickness progression.

2.3 Experimental Dataset

In this study, a subset of the dataset reported by (Orita et al., 2025) is used to evaluate the effectiveness of the proposed approach. In the experiment, participants' body movements were restricted to the seat, resulting in negligible torso and head motion. Participants were seated in a car seat mounted on a linear motion platform that delivered sinusoidal lateral accelerations with a peak of 2 m/s² at 0.3 Hz and a maximum displacement of 3.47 m, alternating with a 1 s stop. The six cycles constituted a one-minute set, and a 5-second stop was inserted between consecutive sets. The maximum number of sets was 16, corresponding to a total motion exposure duration of up to 16 min. Motion sickness was assessed at 1-min intervals during the 5-second stops using the MISC. The motion was terminated either after all 16 sets were completed, when the MISC score reached 6, or upon participant request, followed by six additional post-exposure assessments. Fourteen participants (11 males, 3 females; mean age 24.9 ± 3.4 years) took part in the experiment, and all provided written informed consent in the original study. The experiment was approved by the Ethics Review Committee of Nara Institute of Science and Technology.

2.4 Model Parameters

The SVC part utilizes the same parameters as those employed in the previous study (Inoue et al., 2023, 2025), which are summarized in Table 1. Meanwhile, a set of four parameters for the MISC output part is identified by the proposed method within the allowable ranges depicted in Table 2. In addition to these inequality constraints, the condition $\beta_1 < \beta_2$ is also imposed in the present study. Furthermore, the parameters for the sampling process are selected as $\delta = 5$, $\varepsilon = 0.01$, and $M = 100$. Because Participants 1 and 10 reported zero MISC scores for the entire duration of the experiment; therefore, they were excluded from the analysis.

Table 1. Parameters of the SVC part.

K_a	K_w	K_{wc}	K_{ac}	K_{vc}	τ [s]	τ_d [s]
0.1	0.1	10.0	0.5	5.0	2.0	7.0

Table 2. Allowable ranges for the parameters of the MISC output part.

Parameters	b [m/s ²]	K	β_1 [s]	β_2 [s]
Range of parameter values	[0.05, 50]	[0, 10]	[1, 2000]	[1, 7200]

2.5 Comparative Methods and Data Analysis

The present study compares the proposed method against three alternative strategies, focusing on the mean absolute error (MAE) between observed and predicted MISC values and the number of data points used. Specifically, the four methods considered for comparison are defined as follows:

Proposed method: The adaptive querying strategy described in Section 2.2 was employed.

1-min. interval method: Querying every 1 minute from the onset of motion exposure until the end of the experiment.

2-min. interval method: Querying every 2 minutes from the onset of motion exposure until the end of the experiment.

5-min. interval method: Querying every 5 minutes from the onset of motion exposure until the end of the experiment.

For each method, parameter identification was sequentially performed when a new query was issued, using (1) with the previously observed MISC values. It should be noted that when the interval between two consecutive queries exceeded one minute, the observed MISC values were linearly interpolated using (14) to obtain one-minute-interval data, after which the optimization was performed.

$$\text{MISC}_{int}^{obs}(t) = \frac{\text{MISC}_{k+1}^{obs} - \text{MISC}_k^{obs}}{t_{k+1} - t_k} (t - t_k) + \text{MISC}_k^{obs} \quad t \in [t_k, t_{k+1}) , \quad (14)$$

where MISC_k^{obs} and MISC_{k+1}^{obs} denote the observed MISC values obtained at the k -th and $(k+1)$ -th consecutive queries, conducted at times t_k and t_{k+1} , respectively.

Statistical analysis is performed to evaluate the differences among the methods regarding MAE and the number of data points. The initial step involves testing for the assumption of normality using the Shapiro–Wilk test. Since the data are confirmed to deviate from normality, nonparametric procedures are applied in two stages: First, the main effect of the method factor is assessed using the Friedman test. Then, if significant effects are identified, pairwise comparisons among the four methods are conducted using the Wilcoxon signed-rank test with Holm correction.

3 Results

3.1 Model-Based Personalized Prediction of Motion Sickness

Fig. 3 shows the predicted MISC trajectories and their associated uncertainty for each participant, obtained using parameter sets identified from the data collected by the proposed adaptive-querying method. As illustrated, the predictions are generated in an iterative manner: the computational model continuously predicts future MISC progression based on the currently available data, and model parameters are updated only when the querying condition in (12) or (13) is satisfied. At each such time point, the newly observed MISC value from the immediately preceding measurement is incorporated, and subsequent predictions are generated using the updated parameters. As a result, the predicted MISC progressions consist of successive prediction segments reflecting intermittent measurement updates.

Overall, the predicted MISC captures the main trends of the observed symptom progression across all individuals. Quantitative comparisons with the three fixed-interval methods are summarized in Fig. 4. A Friedman test of the MAE exhibited a statistically significant difference among the four methods due to $\chi(3) = 26.65, p < 0.001$. Subsequently, Wilcoxon signed-rank tests with Holm correction were conducted to compare all pairs of the four methods. The MAE of the 5-min. interval method was significantly larger than that of the proposed method ($z = 2.43, p = 0.030$) and that of the 2-min. interval method ($z = 3.059, p = 0.011$), while no significant differences were found between the proposed method and the 2-min. interval method ($z = 1.51, p = 0.13$). Furthermore, the MAE of the 1-min. interval method was also smaller than those of the proposed method ($z = -2.67, p = 0.031$), 2-min. interval method ($z = -2.67, p = 0.023$), and 5-min. interval method ($z = -3.059, p = 0.013$).

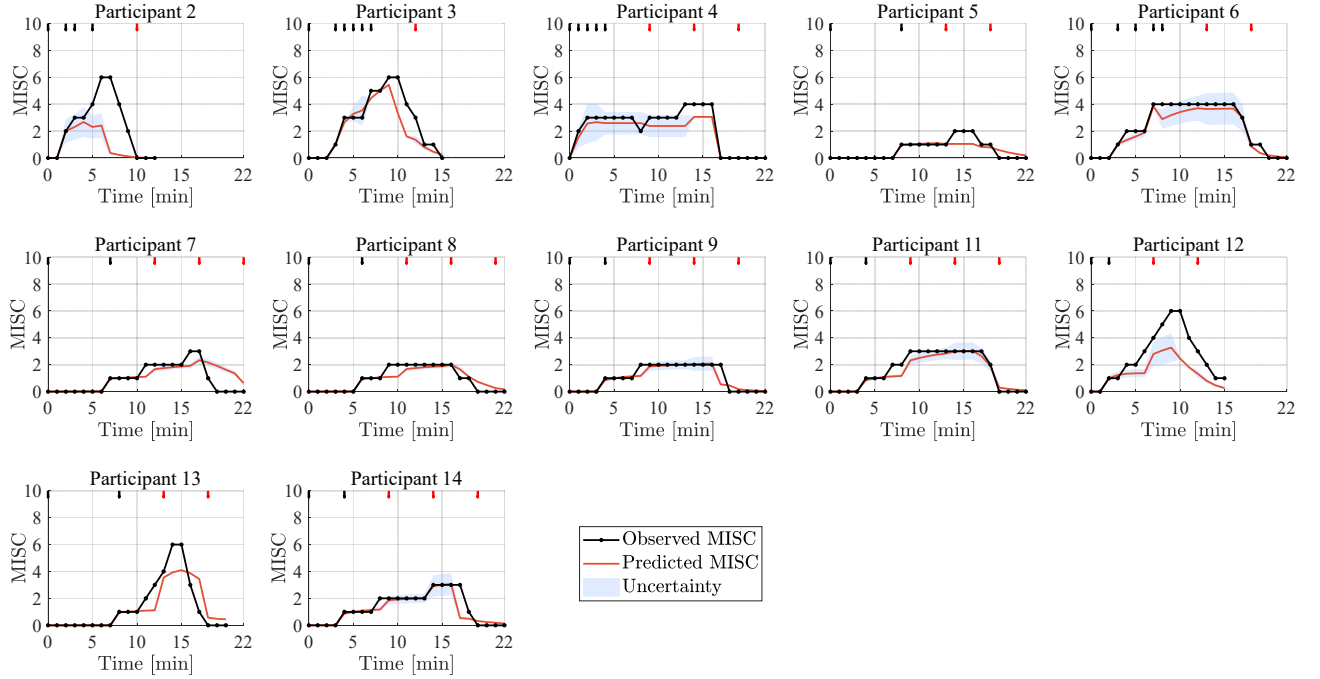


Figure 3. Personalized predicted MISC trajectories and their associated uncertainty, obtained by the proposed method. Although observed MISC values were obtained at 1-min intervals in the original experiment, parameter identification in the proposed method was performed only at time points when queries were issued. At one-minute time points without queries, the observed MISC values were linearly interpolated using (14) and used for parameter identification.

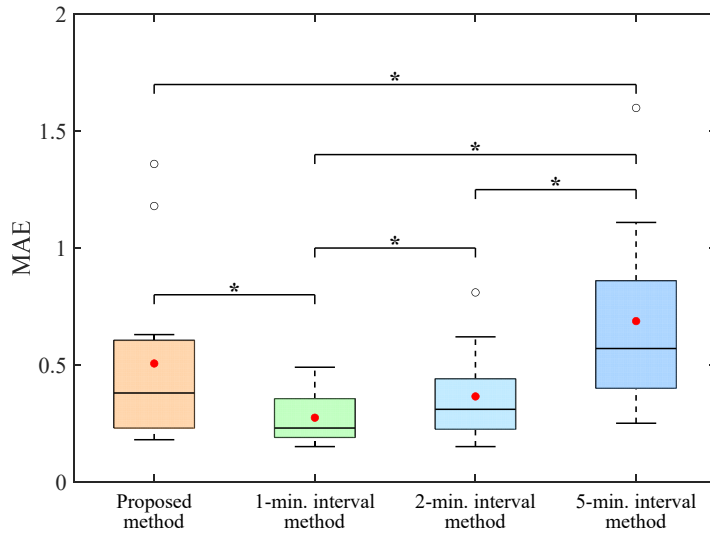


Figure 4. Mean absolute error (MAE) of MISC prediction for each MISC-querying method across individuals. Asterisks indicate statistically significant differences between methods ($*p < 0.05$, $p < 0.01$).**

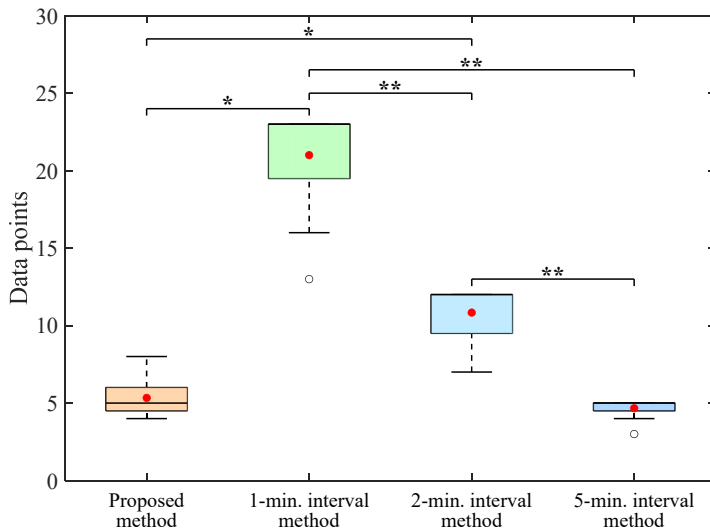


Figure 5. Number of data points used for parameter identification across individuals for each MISC-querying method. Asterisks indicate statistically significant differences between methods ($*p < 0.05$, $p < 0.01$).**

The number of MISC queries used for parameter identification is shown in Fig. 5. A Friedman test of the number of data points revealed a statistically significant main effect of the method ($\chi(3) = 34.21, p < 0.001$). Subsequently, post-hoc Wilcoxon signed-rank tests with Holm correction were conducted. The proposed method used significantly fewer data points than the 1-min interval method ($z = -3.059, p = 0.013$) and the 2-min interval method ($z = -3.059, p = 0.011$), whereas no

significant differences were found between the proposed method and the 5-min. interval method ($z = 1.57, p = 0.12$). The 5-min interval method used significantly fewer data points than the 1-min interval method ($z = -3.059, p = 0.0067$) and the 2-min interval method ($z = -3.059, p = 0.0044$). Moreover, the 1-min interval method used significantly more data points than the 2-min interval method ($z = 3.059, p = 0.0089$).

4 Discussion

4.1 Interpretation of the results

In the present study, we proposed a method that predicts when the MISC score is likely to increase by accounting for model uncertainty, and determines the timing of MISC queries based on this prediction. We then evaluated its effectiveness using a dataset obtained from participants repeatedly exposed to lateral acceleration. The model prediction error (MAE) of the proposed method was significantly larger than that of the 1-min interval method, showed no significant difference from the 2-min interval method, and was significantly smaller than that of the 5-min interval method. Regarding the number of MISC inquiries, no statistically significant difference was observed between the proposed method and the 5-min interval method, whereas the proposed method required significantly fewer queries than the 1-min and 2-min interval methods. These results indicate that the proposed method can achieve a level of prediction accuracy comparable to that of the 2-min interval method, while using a number of MISC queries comparable to the 5-min interval method and fewer queries than both the 1-min and 2-min interval methods.

4.2 Comparison with the existing literature and contribution of the research

In previous studies, severity of sickness or symptom progression such as MISC scores (Bos et al., 2005) have typically been obtained at fixed intervals, such as every one minute (Bos et al., 2005; Kuiper et al., 2020; Reuten et al., 2024; Sato et al., 2026; Wijnens et al., 2024) or 30 seconds (de Winkel et al., 2022; Talsma et al., 2023). This short-interval querying has been used because, in scientific research, the temporal evolution of motion sickness is often unknown a priori, and therefore researchers aim to capture symptom changes as comprehensively as possible. In contrast, engineering applications impose different constraints; frequent querying can be intrusive or annoying for users, and reducing the number of queries is therefore desirable. Reducing the query frequency requires careful consideration of the multifaceted nature of motion sickness. Symptom progression is known to vary markedly as a function of stimulus frequency and amplitude (Donohew & Griffin, 2004; Golding et al., 2001; McCauley et al., 1976). Motion direction also plays an important role: differences relative to the gravity vector and in body-centered coordinates (Golding et al., 1995; Sato et al., 2026) have been shown to influence symptom development. Furthermore, large inter-individual differences are well documented (Golding, 2006; Lackner, 2014), including the frequency range at which symptoms peak (Irmak, de Winkel, et al., 2021). Taking these substantial intra- and inter-individual differences into account, the present study proposed a method that predicts when the MISC score is likely to increase—while incorporating model-prediction uncertainty—and uses this prediction to determine individualized querying timing. Consequently, the proposed method reduces the number of queries while maintaining prediction accuracy. This constitutes the primary contribution of the present research: it demonstrates that an adaptive querying strategy tailored to individual motion sickness dynamics can simultaneously enhance efficiency and preserve model performance. To the best of the authors' knowledge, the present study is the first to address this trade-off and to adaptively adjust the querying timing.

4.3 Limitation and future research directions

The present study has several limitations. First, the validation was conducted using a single dataset obtained under translational motion (Orita et al., 2025), and further investigation is needed to assess how well the proposed method generalizes to different motion profiles—such as variations in frequency, amplitude, and motion direction—as well as to environments including real vehicles. Second, the parameter identification procedure requires non-negligible computation time, and for practical deployment, the development of methods that enable real-time parameter estimation will be essential. Third, the evaluation of symptom progression was limited to the MISC score, and it remains unclear whether the proposed adaptive querying strategy generalizes to other subjective rating scales such as another scale used in (Golding et al., 2003; Wada et al., 2012). Fourth, the present method was examined using a specific SVC-based model; however, as shown in SVC variants such as that of (Kotian et al., 2025), differences in the output stage may influence the performance of the proposed method. Additionally, while model uncertainty was derived from the parameter space in the present study, incorporating noise models or measurement-error distributions may allow future extensions within a Bayesian framework. Furthermore, although the proposed strategy reduces the number of queries, the unpredictability of querying timing itself may impose cognitive burden on users, highlighting the need for improved human-machine interaction design. Finally, the present method did not incorporate prior knowledge regarding individual characteristics. Integrating such information—such as individual susceptibility measured by the Motion Sickness Susceptibility Questionnaire (MSSQ) (Golding, 2006) or known symptom patterns—may further enhance prediction accuracy, particularly during the early stages of exposure.

4.4 Concluding remarks

In this study, we proposed a method that adaptively adjusts the querying timing of subjective sickness progression based on a computational model of sickness and its associated uncertainty, so as to reduce the number of queries while maintaining monitoring accuracy. The results confirmed that this approach achieves substantial reductions in query frequency without degrading predictive performance. This capability is practically important for applications in which excessive querying imposes cognitive or operational burdens, and underscores the value of adaptive symptom-monitoring strategies.

Conflict of Interest

The authors declare that the research was conducted in the absence of any commercial or financial relationships that could be construed as a potential conflict of interest.

Author Contributions

Conceptualization: TW; Methodology: VD, TW; Formal analysis and investigation: VD, TW; Writing – original draft preparation: TW, VD; Writing - review and editing: TW, VD.

Funding

This work was partially supported by the JSPS KAKENHI (Grant number 24H00298).

Data Availability Statement

The data supporting the conclusions of this article will be made available by the authors, without undue reservation.

359

360

361 **References**

- 362 Bles, W., Bos, J. E., de Graaf, B., Groen, E., & Wertheim, A. H. (1998). Motion Sickness: Only One
363 Provocative Conflict? *Brain Research Bulletin*, 47(5), 481–487.
- 364 Bos, J. E., & Bles, W. (1998). Modeling Motion Sickness and Subjective Vertical Mismatch Detailed
365 for Vertical Motions. *Brain Research Bulletin*, 47(5), 537–542.
- 366 Bos, J. E., & Bles, W. (2002). Theoretical considerations on canal-otolith interaction and an observer
367 model. *Biological Cybernetics*, 86(3), 191–207. <https://doi.org/10.1007/s00422-001-0289-7>
- 368 Bos, J. E., Bles, W., & Dallinga, R. (2002). Prediction of Seasickness with More Than One Degree of
369 Freedom. *Human Factors in Ship Design and Operation*, 57–62.
- 370 Bos, J. E., MacKinnon, S. N., & Patterson, A. (2005). Motion sickness symptoms in a ship motion
371 simulator: effects of inside, outside, and no view. *Aviation, Space, and Environmental Medicine*,
372 76(12), 1111–1118. <http://www.ncbi.nlm.nih.gov/pubmed/16370260>
- 373 Bos, J. E., Souman, J. L., Nooij, S., & Diels, C. (2024). Advancing ISO 2631-1 by considering pre-
374 emesis symptoms in carsickness. *Proceedings of Driving Simulator Conference Europe*.
- 375 Braccesi, C., Cianetti, F., & Elia, A. (2011). Motion sickness. Part I: development of a model for
376 predicting motion sickness incidence. *International Journal of Human Factors Modelling and*
377 *Simulation*, 2(3), 163–187. <https://doi.org/10.1504/IJHFMS.2011.044494>
- 378 de Winkel, K. N., Irmak, T., Kotian, V., Pool, D. M., & Happee, R. (2022). Relating individual
379 motion sickness levels to subjective discomfort ratings. *Experimental Brain Research*, 240(4),
380 1231–1240. <https://doi.org/10.1007/s00221-022-06334-6>
- 381 Diels, C., & Bos, J. E. (2016). Self-driving carsickness. *Applied Ergonomics*, 53, 374–382.
382 <https://doi.org/10.1016/j.apergo.2015.09.009>
- 383 Donohew, B. E., & Griffin, M. J. (2004). Motion Sickness: Effect of the Frequency of Lateral
384 Oscillation. *Aviation, Space, and Environmental Medicine*.
- 385 Golding, J. F. (2006). Predicting individual differences in motion sickness susceptibility by
386 questionnaire. *Personality and Individual Differences*, 41(2), 237–248.
387 <https://doi.org/10.1016/j.paid.2006.01.012>
- 388 Golding, J. F., Bles, W., Bos, J. E., Haynes, T., & Gresty, M. A. (2003). Motion sickness and tilts of
389 the inertial force environment: active suspension systems vs. active passengers. *Aviation, Space,*
390 *and Environmental Medicine*, 74(3), 220–227. <http://www.ncbi.nlm.nih.gov/pubmed/12650268>
- 391 Golding, J. F., & Gresty, M. A. (2005). Motion sickness. *Current Opinion in Neurology*, 18(1), 29–
392 34. <https://doi.org/10.1097/00019052-200502000-00007>

- 393 Golding, J. F., Markey, H. M., & Stott, J. R. (1995). The effects of motion direction, body axis, and
394 posture on motion sickness induced by low frequency linear oscillation. *Aviation, Space, and*
395 *Environmental Medicine*, 66(11), 1046–1051. <http://www.ncbi.nlm.nih.gov/pubmed/8588793>
- 396 Golding, J. F., Mueller, A. G., & Gresty, M. A. (2001). A motion sickness maximum around the 0.2
397 Hz frequency range of horizontal translational oscillation. *Aviation, Space, and Environmental*
398 *Medicine*, 72(3), 188–192. <http://www.ncbi.nlm.nih.gov/pubmed/11277284>
- 399 Inoue, S., Dang, V. T., Liu, H., & Wada, T. (2025). Construction of a computational model of
400 individual progression of motion sickness symptoms based on subjective vertical conflict
401 theory. *Experimental Brain Research*, 243(5), 108. <https://doi.org/10.1007/s00221-025-07052-5>
- 402 Inoue, S., Liu, H., & Wada, T. (2023, April 11). Revisiting Motion Sickness Models Based on SVC
403 Theory Considering Motion Perception. *SAE Technical Paper*. [https://doi.org/10.4271/2023-01-](https://doi.org/10.4271/2023-01-0176)
404 0176
- 405 Inoue, S., Liu, H., & Wada, T. (2024). A Digital Human Model for Symptom Progression of
406 Vestibular Motion Sickness based on Subjective Vertical Conflict Theory. *2024 AHFE*
407 *International Conference on Human Factors in Design, Engineering, and Computing*.
- 408 Irmak, T., de Winkel, K. N., Pool, D. M., Bülthoff, H. H., & Happee, R. (2021). Individual motion
409 perception parameters and motion sickness frequency sensitivity in fore-aft motion.
410 *Experimental Brain Research*, 239(6), 1727–1745. <https://doi.org/10.1007/s00221-021-06093-w>
- 411 Irmak, T., Kotian, V., Happee, R., de Winkel, K. N., & Pool, D. M. (2022). Amplitude and Temporal
412 Dynamics of Motion Sickness. *Frontiers in Systems Neuroscience*, 16.
413 <https://doi.org/10.3389/fnsys.2022.866503>
- 414 Irmak, T., Pool, D. M., & Happee, R. (2021). Objective and subjective responses to motion sickness:
415 the group and the individual. *Experimental Brain Research*, 239(2), 515–531.
416 <https://doi.org/10.1007/s00221-020-05986-6>
- 417 ISO2631-1. (1997). *Mechanical Vibration and Shock –Evaluation of Human Exposure to Whole-*
418 *body Vibration- Part1*. International Organization for Standardization.
- 419 Kamiji, N., Kurata, Y., Wada, T., & Doi, S. (2007). Modeling and validation of carsickness
420 mechanism. *Proceedings of International Conference on Instrumentation, Control and*
421 *Information Technology*, 1138–1143.
- 422 Kotian, V., Pool, D. M., & Happee, R. (2023). Modelling individual motion sickness accumulation in
423 vehicles and driving simulators. *Proceedings of the 22nd Driving Simulation & Virtual Reality*
424 *Conference*.
- 425 Kotian, V., Pool, D. M., & Happee, R. (2025). Personalizing motion sickness models: estimation and
426 statistical modeling of individual-specific parameters. *Frontiers in Systems Neuroscience*, 19.
427 <https://doi.org/10.3389/fnsys.2025.1531795>
- 428 Kuiper, O. X., Bos, J. E., Diels, C., & Schmidt, E. A. (2020). Knowing what’s coming: Anticipatory
429 audio cues can mitigate motion sickness. *Applied Ergonomics*, 85(July 2019), 103068.
430 <https://doi.org/10.1016/j.apergo.2020.103068>

- 431 Kuiper, O. X., Bos, J. E., Schmidt, E. A., Diels, C., & Wolter, S. (2019). Knowing What's Coming:
 432 Unpredictable Motion Causes More Motion Sickness. *Human Factors: The Journal of the*
 433 *Human Factors and Ergonomics Society*, 62(8), 1339–1348.
 434 <https://doi.org/10.1177/0018720819876139>
- 435 Lackner, J. R. (2014). Motion sickness: More than nausea and vomiting. *Experimental Brain*
 436 *Research*, 232(8), 2493–2510. <https://doi.org/10.1007/s00221-014-4008-8>
- 437 Liu, H., Inoue, S., & Wada, T. (2024). Subjective Vertical Conflict Model With Visual Vertical:
 438 Predicting Motion Sickness on Autonomous Personal Mobility Vehicles. *IEEE Transactions on*
 439 *Intelligent Transportation Systems*, 25(8), 9878–9894.
 440 <https://doi.org/10.1109/TITS.2024.3357170>
- 441 McCauley, M. E., Royal, J. W., Wylie, C. D., O'Hanlon, J. F., & Mackie, R. R. (1976). Motion
 442 Sickness Incidence: Exploratory Studies of Habituation, Pitch and Roll, and the Refinement of a
 443 Mathematical Model. *Technical Report 1733-2, Human Factors Research Inc., Santa Barbara*
 444 *Research Park, Goleta, California, USA*.
 445 <http://oai.dtic.mil/oai/oai?verb=getRecord&metadataPrefix=html&identifier=ADA024709>
- 446 Oman, C. M. (1982). A heuristic mathematical model for the dynamics of sensory conflict and
 447 motion sickness. *Acta Oto-Laryngologica. Supplementum*, 392, 1–44.
 448 <http://www.ncbi.nlm.nih.gov/pubmed/6303041>
- 449 Oman, C. M. (1990). Motion sickness: a synthesis and evaluation of the sensory conflict theory.
 450 *Canadian Journal of Physiology and Pharmacology*, 68(2), 294–303.
 451 <https://doi.org/10.1139/y90-044>
- 452 Orita, Y., Sato, E., Wada, T., Kida, S., Horita, H., Rakumatsu, T., Yamagata, Y., & Yamaguchi, K.
 453 (2025). Preliminary Report on the Effects of Shoulder Motion Restriction on Motion Sickness
 454 Under Lateral Acceleration Conditions in Darkness. *Zenodo*.
 455 <https://doi.org/10.5281/zenodo.14673317>
- 456 Reason, J. T. (1978). Motion Sickness Adaptation: A Neural Mismatch Model. *Journal of the Royal*
 457 *Society of Medicine*, 71(11), 819–829. <https://doi.org/10.1177/014107687807101109>
- 458 Reuten, A. J. C., Yunus, I., Bos, J. E., Martens, M. H., & Smeets, J. B. J. (2024). Anticipatory cues
 459 can mitigate car sickness on the road. *Transportation Research Part F: Traffic Psychology and*
 460 *Behaviour*, 105, 196–205. <https://doi.org/10.1016/j.trf.2024.07.006>
- 461 Sato, E., Kajita, K., Ito, K., & Wada, T. (2026). Anisotropy in motion sickness susceptibility during
 462 longitudinal and lateral motion while seated on a car seat. *Applied Ergonomics*, 130, 104664.
 463 <https://doi.org/10.1016/J.APERGO.2025.104664>
- 464 Sivak, M., & Schoettle, B. (2015). Motion Sickness in Self-driving Vehicles. In *UMTRI Technical*
 465 *Report: Vol. UMTRI-2015*.
- 466 Talsma, T. M. W., Hassanain, O., Happee, R., & de Winkel, K. N. (2023). Validation of a moving
 467 base driving simulator for motion sickness research. *Applied Ergonomics*, 106, 103897.
 468 <https://doi.org/10.1016/j.apergo.2022.103897>

- Tamura, Y., Wada, T., & Liu, H. (2023). Generating Visual Information for Motion Sickness Reduction Using a Computational Model Based on SVC Theory. *2023 IEEE 26th International Conference on Intelligent Transportation Systems (ITSC)*, 5066–5071. <https://doi.org/10.1109/ITSC57777.2023.10422244>
- Wada, T. (2016). Motion Sickness in Automated Vehicles. In G. Meyer & S. Beiker (Eds.), *International Symposium on Advanced Vehicle Control*. Springer International Publishing. <https://doi.org/10.1007/978-3-319-40503-2>
- Wada, T. (2021). Computational Model of Motion Sickness Describing the Effects of Learning Exogenous Motion Dynamics. *Frontiers in Systems Neuroscience*, 15. <https://doi.org/10.3389/fnsys.2021.634604>
- Wada, T., & Bos, J. E. (2025). Theoretical considerations on models of vestibular self-motion perception as inherent in computational frameworks of motion sickness. *Biological Cybernetics*, 119(4–6), 22. <https://doi.org/10.1007/s00422-025-01018-0>
- Wada, T., Fujisawa, S., & Doi, S. (2018). Analysis of driver's head tilt using a mathematical model of motion sickness. *International Journal of Industrial Ergonomics*, 63, 89–97. <https://doi.org/10.1016/j.ergon.2016.11.003>
- Wada, T., Kawano, J., Okafuji, Y., Takamatsu, A., & Makita, M. (2020). A Computational Model of Motion Sickness Considering Visual and Vestibular Information. *2020 IEEE International Conference on Systems, Man, and Cybernetics (SMC)*, 1758–1763. <https://doi.org/10.1109/SMC42975.2020.9283350>
- Wada, T., Konno, H., Fujisawa, S., & Doi, S. S. (2012). Can Passengers' Active Head Tilt Decrease the Severity of Carsickness?: Effect of Head Tilt on Severity of Motion Sickness in a Lateral Acceleration Environment. *Human Factors: The Journal of the Human Factors and Ergonomics Society*, 54(2), 226–234. <https://doi.org/10.1177/0018720812436584>
- Wijlens, R., Englebert, B. J. V., Takamatsu, A., Makita, M., Sato, H., Wada, T., de Winter, J. C. F., van Paassen, M. M., & Mulder, M. (2024). On the road to comfort: Evaluating the influence of motion predictability on motion sickness in automated vehicles. *Ergonomics*, 1–19. <https://doi.org/10.1080/00140139.2024.2372704>
- Yunus, I., Jerrelind, J., & Drugge, L. (2022). *Evaluation of Motion Sickness Prediction Models for Autonomous Driving* (pp. 875–887). https://doi.org/10.1007/978-3-031-07305-2_81
- Yunus, I., Papaioannou, G., Jerrelind, J., & Drugge, L. (2025). A Review of Vehicle Dynamics and Control Approaches for Mitigating Motion Sickness in Autonomous Vehicles. *IEEE Access*, 13, 132990–133024. <https://doi.org/10.1109/ACCESS.2025.3592407>